RAD Conference Proceedings, vol. 9, pp. 19-25, 2025
ISSN 2466-4626 (online) | DOI: 10.21175/RadProc.2025.04
www.rad-proceedings.org

# LENGTHWISE FRACTURE ANALYSIS OF INHOMOGENEOUS FRAMES AT CREEP

**Victor Rizov***

University of Architecture, Civil Engineering and Geodesy, Sofia, Bulgaria

***Abstract***. *The present paper examines the lengthwise fracture of a continuously inhomogeneous portal frame by analyzing the time-dependent strain energy release rate (SERR). The frame is subjected to creep. The material of the frame has inhomogeneity in both thickness and width directions of the cross-section. The mechanical behavior of the material is treated by applying a non-linear stress-strain-time relationship. A solution to the SERR is derived assuming that the material properties involved in the non-linear stress-strain-time relationship vary continuously along the width and the thickness of the frame cross-section. The SERR is derived also by considering the complementary strain energy (CSE) for verification. The solution is applied to evaluate the variation of the SERR over the time. It is investigated how the material inhomogeneity along the width and the thickness of the frame affects the SERR.*

**Keywords:** *Frame, Lengthwise Fracture, Inhomogeneous Structure, Non-linear Stress-strain-time Relationship*

## 1. INTRODUCTION

The material properties of continuously inhomogeneous structural members and components vary smoothly in the solid. Now the continuously inhomogeneous structural materials occupy an established position in aeronautics, automotive industry, nuclear reactors and civil infrastructure. A typical example for such materials is functionally graded materials whose properties can be tailored during the manufacturing process with aim of satisfying different performance requirements in different part of a structural member [1], [2]. It should be mentioned that the importance of functionally graded materials for the modern engineering constantly increases [3], [4]. Thus, it is not surprising that more attention has been paid from the international research community to continuously inhomogeneous (functionally graded) materials and structures in the recent decades [5], [6]. Numerical methods, such as the finite element method, have also been used to study the response of these advanced materials to various loadings [7], [8], [9].

The fracture behavior has a fundamental influence on the load-bearing capacity, integrity, reliability and durability of the continuously inhomogeneous structural members and components. Being different from the traditional homogeneous materials, the fracture analysis of continuously inhomogeneous (functionally graded) materials posses some specific characteristics, the most important of which is the fact that the material properties are related to coordinates [10].

Another factor of great importance for the fracture is the creep behavior of inhomogeneous materials [11], [12], [13].

Influence of creep behavior on fracture in a functionally graded material is researched in [11]. A material with power law constitutive equation is considered. Effect of elevated temperature on the crack is studied. The crack resistance capability under creep is evaluated. A parametric investigation of fracture is performed.

Creep fracture behavior of pressure vessel with a semielliptical crack is studied in [12]. The creep crack propagation is considered. A detailed evaluation of the influence of creep behavior on the fracture and structural integrity is performed.

Important experimental investigations throwing light on the influence of creep behavior on fracture in a functionally graded material are reported in [13]. The creep crack tests on specimens produced by hot-pressing method are carried-out under constant loading.

Inhomogeneous (functionally graded) structural elements and components are very often built layer by layer. This manufacturing process, however, has one basic disadvantage, namely the relatively weak adhesion between layers which results in emergence of lengthwise cracks [14], [15]. This fact indicates clearly that lengthwise fracture of continuously inhomogeneous structural members is worth to explore. The present paper analyzes the lengthwise fracture of an inhomogeneous frame structure under creep. The analysis is motivated by the fact that load-bearing inhomogeneous frame structures are widely used in various areas of modern engineering. Here, a solution of the SERR is derived by analyzing the balance of energy (BE). For verification purposes, SERR is also obtained through CSE analysis. The integral $J$ also is used for verification. Since the crack is located inside the frame structure, the bending moments in the arms of the crack which are used to obtain the SERR are determined by treating the frame as a structure with one degree of internal static indeterminacy. The novelty of the present research is that a continuously inhomogeneous frame structure hosting an internal lengthwise crack under creep is analyzed. The same way for analysis can be applied to

* E-mail of the corresponding author: v_rizov_fhe@uacg.bg

lengthwise fracture in frame structures with different geometry, loading, boundary conditions, crack location, stress-strain-time relationship, and material properties distribution laws.

## 2. Model for analysis of SERR

A continuously inhomogeneous portal frame that consists of two vertical columns, $AC$ and $DH$, of length, $l$, and a horizontal bar, $CD$, also of length, $l$, is under consideration (Fig. 1). The horizontal bar and the vertical columns are rigidly attached at $C$ and $D$. The bar and the columns have a section with width, $b$, and thickness, $h$.

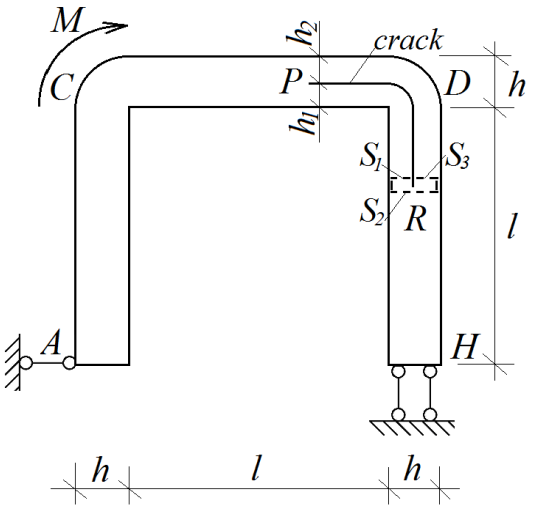


Figure 1. Geometry and loading of inhomogeneous portal frame with a lengthwise crack

The frame is under bending moment, $M$, in point, $C$, as shown in Fig. 1. The frame is supported by a roller in section, $A$, and a $Q$-apparatus in section, $H$. Thus, the frame support conditions are as follows: zero horizontal displacement of section, $A$, and zero vertical displacement and rotation of section, $H$. Under these support conditions, the moment, $M$, induces only one non-zero support reaction, namely the moment in $Q$-apparatus in section, $H$. It is obvious that column, $AC$, is free of stresses. The horizontal bar and column, $DH$, are loaded in pure bending. A lengthwise crack, $PR$, of length, $2a$, is located in bar, $CD$, and in column, $DH$, symmetrically with respect to $D$. The thickness of the inner and the outer arms of the crack are $h_1$ and $h_2$, respectively.

The frame material exhibits creep behavior, which is treated by the stress-strain-time relationship described below [10]:

$$\varepsilon=\frac{\sigma}{E}+B_1\sigma^m+B_2\sigma^m t+B_3\sigma^m\left(1-e^{-\beta t}\right), \qquad (1)$$

where $\varepsilon$ is the longitudinal strain, $\sigma$ is the normal stress, $E$ is the elasticity modulus, $B_1$, $B_2$, $B_3$, $m$ and $\beta$ are material properties, $t$ is the time. The first and the second terms of the right-hand side of equation (1) describe the instantaneous linear-elastic and plastic strains, respectively. The creep strain is described by the third and the fourth terms (the third term is the steady-state creep strain, while the fourth is the transient creep strain).

The frame has continuous (smooth) material inhomogeneity in both width and thickness directions of its cross-section. Thus, the distributions of $E$, $B_1$, $B_2$, $B_3$, $m$ and $\beta$ are expressed as

$$E=E_l+\frac{E_d-E_l}{b^n}\left(\frac{b}{2}+y_4\right)^n+\frac{E_g-E_l}{h^f}\left(\frac{h}{2}+z_4\right)^f, \qquad (2)$$

$$B_1=B_{1l}+\frac{B_{1d}-B_{1l}}{b^{n_1}}\left(\frac{b}{2}+y_4\right)^{n_1}+\frac{B_{1g}-B_{1l}}{h^{f_1}}\left(\frac{h}{2}+z_4\right)^{f_1}, \qquad (3)$$

$$B_2=B_{2l}+\frac{B_{2d}-B_{2l}}{b^{n_2}}\left(\frac{b}{2}+y_4\right)^{n_2}+\frac{B_{2g}-B_{2l}}{h^{f_2}}\left(\frac{h}{2}+z_4\right)^{f_2}, \qquad (4)$$

$$B_3=B_{3l}+\frac{B_{3d}-B_{3l}}{b^{n_3}}\left(\frac{b}{2}+y_4\right)^{n_3}+\frac{B_{3g}-B_{3l}}{h^{f_3}}\left(\frac{h}{2}+z_4\right)^{f_3}, \qquad (5)$$

$$m=m_l+\frac{m_d-m_l}{b^{n_m}}\left(\frac{b}{2}+y_4\right)^{n_m}+\frac{m_g-m_l}{h^{f_m}}\left(\frac{h}{2}+z_4\right)^{f_m}, \qquad (6)$$

$$\beta=\beta_l+\frac{\beta_d-\beta_l}{b^{n_\beta}}\left(\frac{b}{2}+y_4\right)^{n_\beta}+\frac{\beta_g-\beta_l}{h^{f_\beta}}\left(\frac{h}{2}+z_4\right)^{f_\beta}, \qquad (7)$$

where $E_l$, $E_d$, $E_g$, $n$ and $f$ are material properties ($E_d$ and $E_g$ control the distribution of the modulus of elasticity in the width and the thickness directions, respectively), $y_4$ and $z_4$ are the centroidal axes of the cross-section. In (3), $B_{1l}$, $B_{1d}$, $B_{1g}$, $n_1$ and $f_1$ are material properties (the distribution of $B_1$ along the width and thickness of the cross-section is controlled

by $B_{1d}$ and $B_{1g}$, respectively). The properties, $B_{2d}$ and $B_{2g}$, which are involved in (4), control the distribution of $B_2$ in the width and thickness directions, respectively. The distribution of $B_3$ in the width and thickness directions is controlled, respectively, by $B_{3d}$ and $B_{3g}$ (refer to (5)). In (6), the properties, $m_d$ and $m_g$, control the distribution of $m$ in the width and thickness directions, respectively. The distribution of $\beta$ in the width and the thickness directions is controlled by $\beta_d$ and $\beta_g$, respectively.

Since symmetry is present, only the horizontal bar, $CD$, is studied. The SERR, $G$, is derived by analyzing the BE in the frame. For this purpose, the BE is written as given below

$$M\delta\varphi=\frac{\partial U}{\partial a}\delta a+Gb\delta a\,, \tag{8}$$

where $\varphi$ is the rotation angle, $U$ is the strain energy (SE) and $\delta a$ is a small growth of the delamination. Form (8), one derives

$$G=2\left(\frac{M}{b}\frac{\partial\varphi}{\partial a}-\frac{1}{b}\frac{\partial U}{\partial a}\right). \tag{9}$$

Since symmetry is present, expression (9) is multiplied by 2.

The rotation angle, $\varphi$, is determined by applying the theorem of Castigliano for structures with material non-linearity

$$\varphi=\frac{\partial U^*}{\partial M}\,, \tag{10}$$

where $U^*$ is the CSE cumulated in the horizontal bar. The quantity, $U^*$, is written as

$$U^*=U_1^*+U_2^*+U_3^*\,, \tag{11}$$

where $U_1^*$, $U_2^*$ and $U_3^*$ are the CSE in the inner and the outer arms of the crack, and in the un-cracked portion, $CP$, of the horizontal bar.

The CSE in the inner arm of the crack is

$$U_1^*=a\iint\limits_{(A_1)}u_{01}^*dA\,, \tag{12}$$

where $A_1$ is the area and $u_{01}^*$ is the CSE density. The quantity, $u_{01}^*$, is obtained as [8]

$$u_{01}^*=\sigma\varepsilon-u_{01}\,, \tag{13}$$

where $u_{01}$ is the strain energy density, expressed as

$$u_{01}=\int\limits_0^{\varepsilon}\sigma d\varepsilon\,. \tag{14}$$

By combing of (1) and (14), $u_{01}$ is found as

$$u_{01}=\frac{\sigma^2}{2E}+\frac{B_1\sigma^{m+1}m}{m+1}+\frac{B_2\sigma^{m+1}mt}{m+1}+\frac{B_3\sigma^{m+1}m\left(1-e^{-\beta t}\right)}{m+1}\,. \tag{15}$$

By using of (1), (13) and (15), the CSE density is obtained as

$$u_{01}^*=\frac{\sigma^2}{2E}+\frac{B_1\sigma^{m+1}}{m+1}+\frac{B_2\sigma^{m+1}t}{m+1}+\frac{B_3\sigma^{m+1}\left(1-e^{-\beta t}\right)}{m+1}\,. \tag{16}$$

The distribution of the strain that is involved in (1) is treated by formula (19), i.e.

$$\varepsilon=\varepsilon_{C_1}+\kappa_{y_1}y_1+\kappa_{z_1}z_1\,, \tag{17}$$

where $\varepsilon_{C_1}$ is the strain in the centre of the cross-section, $\kappa_{y_1}$ and $\kappa_{z_1}$ are the curvatures of the inner arm of the crack in the $x_1y_1$ and $x_1z_1$ planes, respectively. Linear distribution (17) of strains is acceptable here since the frame is subjected to pure bending. The same distribution can be applied in cases when frames are under bending moment and shear force if the frame members have high aspect ratios (i.e., high length to thickness ratios). The distribution of the strains in the outer arm of the crack is expressed by replacing of $\varepsilon_{C_1}$, $\kappa_{y_1}$, $\kappa_{z_1}$, $y_1$ and $z_1$ with $\varepsilon_{C_2}$, $\kappa_{y_2}$, $\kappa_{z_2}$, $y_2$ and $z_2$ in (17) where $\varepsilon_{C_2}$ is the strain in the center, $\kappa_{y_2}$ and $\kappa_{z_2}$ are the curvatures in the $x_2y_2$ and $x_2z_2$ planes ($x_2$, $y_2$ and $z_2$ are the centric axes of the outer arm). Here, $\varepsilon_{C_1}$, $\kappa_{y_1}$, $\kappa_{z_1}$, $\varepsilon_{C_2}$, $\kappa_{y_2}$ and $\kappa_{z_2}$ are determined by using the equations

$$N_1=\iint\limits_{(A_1)}\sigma dA\,, \tag{18}$$

$$M_{y_1}=\iint\limits_{(A_1)}\sigma z_1dA\,, \tag{19}$$

$$M_{z_1}=\iint\limits_{(A_1)}\sigma y_1dA\,, \tag{20}$$

$$N_2=\iint\limits_{(A_2)}\sigma_\beta dA\,, \tag{21}$$

$$M_{y_2}=\iint\limits_{(A_2)}\sigma_\beta z_2dA\,, \tag{22}$$

$$M_{z_2}=\iint\limits_{(A_2)}\sigma_\beta y_2dA\,, \tag{23}$$

where $N_1$, $M_{y_1}$ and $M_{z_1}$ are the axial force and the moments with respect to centric axes, $y_1$ and $z_1$, of the inner arm of crack (it is obvious that $N_1=0$ and $M_{z_1}=0$), $N_2$, $M_{y_2}$ and $M_{z_2}$ are the axial force and the moments with respect to centric axes,

$y_2$ and $z_2$, of the outer arm of the crack (obviously, $N_2=0$ and $M_{z_2}=0$), $A_1$ and $A_2$ are the areas of the inner and the outer arms, $\sigma$ and $\sigma_\beta$ are normal stresses in the inner and the outer arms.

For the moments, we can write

$$M_{y_1}+M_{y_2}=M. \quad (24)$$

A further one equation is obtained by treating the frame as a structure with one degree of internal static indeterminacy (the moment, $M_{y_2}$, is taken as a hyperstatic unknown). The statically undetermined problem is solved by applying the theorem of Castigliano for structures with material non-linearity

$$\frac{dU^*_{PD}}{dM_{y_2}}=0. \quad (25)$$

The CSE in the un-cracked portion, $CP$, of the horizontal bar does not depend on $M_{y_2}$ (Fig. 1). Therefore, only the CSE, $U^*_{PD}$, in the two arms of the crack arms in portion, $PD$, of the horizontal bar is involved in (25). Thus, $U^*_{PD}$ is written as

$$U^*_{PD}=U^*_1+U^*_2. \quad (26)$$

The CSE in the outer arm of the crack is

$$U^*_2=a\iint\limits_{(A_2)}u^*_{02}dA, \quad (27)$$

where the CSE density, $u^*_{02}$, is found by replacing of $\sigma$ with $\sigma_\beta$ in (18). Equations (18) – (25) are solved with respect to $\varepsilon_{C_1}$, $\kappa_{y_1}$, $\kappa_{z_1}$, $\varepsilon_{C_2}$, $\kappa_{y_2}$, $\kappa_{z_2}$, $M_{y_1}$ and $M_{y_2}$ using the MatLab by the Newton-Raphson method.

The SE in the horizontal bar is found by applying formula (11). For this purpose, $U^*_1$, $U^*_2$ and $U^*_3$ are replaced with $U_1$, $U_2$ and $U_3$. Here, $U_1$, $U_2$ and $U_3$ are the SE in the inner and the outer arms, and in the un-cracked portion, $CP$, of the horizontal bar. The SE, $U_1$ and $U_2$, are found by applying formulae (12) and (27), respectively. For this purpose, $u^*_{01}$ and $u^*_{02}$ are replaced with $u_{01}$ and $u_{02}$. The SE density, $u_{02}$, in the outer arm is calculated by replacing of $\sigma$ with $\sigma_\beta$ in (15). The SE in the un-cracked portion, $CP$, of the horizontal bar is written as

$$U_3=(l-a)\iint\limits_{(A_3)}u_{03}dA, \quad (28)$$

where $A_3$ is the area the horizontal bar, $u_{03}$ is the SE density. Formula (15) is used to obtain $u_{03}$. For this purpose, $\sigma$ is replaced with $\sigma_\delta$ where $\sigma_\delta$ is the normal stress in un-cracked portion, $CP$, of the horizontal bar. The strain in the centre and the curvatures of portion, $CP$, of the horizontal bar are determined by using equations (18), (19) and (20). For this purpose, $M_{y_1}$, $A_1$, $\sigma$ and $z_1$ are replaced with $M$, $A_3$, $\sigma_\delta$ and $z_3$ where $z_3$ is vertical axis of the horizontal bar.

By substituting of (10), (11), (12), (27) and (28) in (9), one obtains

$$G=\frac{2}{b}\left[M\frac{\partial}{\partial M}\left(\iint\limits_{(A_1)}u^*_{01}dA+\iint\limits_{(A_2)}u^*_{02}dA\right)-\iint\limits_{(A_1)}u_{01}dA-\iint\limits_{(A_2)}u_{02}dA+\iint\limits_{(A_3)}u_{03}dA\right]. \quad (29)$$

where the derivative, $\frac{\partial}{\partial M}(..)$, is found numerically by the MatLab using the finite difference method. The integration in (29) is performed by MatLab (a Gaussian quadrature integration scheme is adopted).

In order to verify (29), the SERR is obtained also by applying the formula [16]

$$G=\frac{2}{b}\left(\iint\limits_{(A_1)}u^*_{01}dA+\iint\limits_{(A_2)}u^*_{02}dA+\iint\limits_{(A_3)}u^*_{03}dA\right). \quad (30)$$

Since symmetry is present, the above expression is multiplied by 2. The MatLab is used for the integration in (30). The SERR found by (30) is exact match of that obtained by (29) which is a verification of the solution. Expressions (29) and (30) can be used to calculate SERR for any specific time, $t$, since CSE and SE densities are continuous functions of time according to formulas (15) and (16).

Another check of (29) is performed by the $J$-integral method [17]. By using the contour, $S_1S_2S_3$, the solution of $J$-integral is found as

$$J=2(J_{S1}+J_{S2}+J_{S3}). \quad (31)$$

The three quantities in the brackets in (31) are the solutions in the three segments of the contour shown in Fig. 1. The quantity, $J_{S1}$, is obtained by (32).

$$J_{S1}=\frac{1}{b}\int\limits_{-\frac{b}{2}}^{\frac{b}{2}}\left\{\int\limits_{S_1}\left[u_{01}\cos\alpha-\left(p_x\frac{\partial u}{\partial x}+p_y\frac{\partial v}{\partial x}\right)\right]ds\right\}dy_1 \quad (32)$$

.

The expressions for $J_{S2}$ and $J_{S3}$ are determined in analogical way. The solution of the $J$-integral matches the SERR, which is another check.

3. PARAMETRIC INVESTIGATION

In this section of the paper, results of a parametric investigation of the lengthwise fracture in the continuously inhomogeneous portal frame subjected to creep are presented. For this purpose, the time-dependent solution to the SERR (29) is applied. The SERR is in a non-dimensional form. In this relation, the formula $G_N = G/(E_l b)$ is used. One of the objectives of the parametric study is to evaluate how time affects longitudinal failure in the frame.

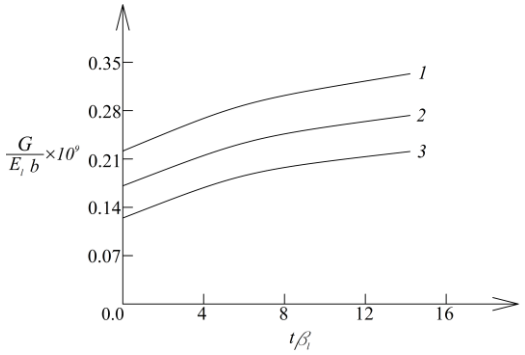


Figure 2. The non-dimensional SERR versus the non-dimensional time (curve 1 - at $E_d / E_l = 0.5$ , curve 2 – at $E_d / E_l = 1.0$ and curve 3 - at $E_d / E_l = 2.0$ )

The influence of the continuous material inhomogeneity in the width and thickness directions of the cross-section on the lengthwise fracture in the frame is also evaluated. It is assumed that $b = 0.010$ m, $h = 0.015$ m, $l = 0.500$ m and $M = 4$ Nm.

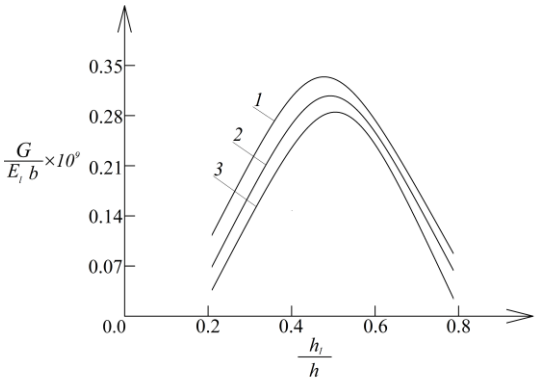


Figure 3. The non-dimensional SERR versus $h_1 / h$ ratio (curve 1 - at $E_g / E_l = 0.5$ , curve 2 - at $E_g / E_l = 1.0$ and curve 3 - at $E_g / E_l = 2.0$ )

The values of other parameters of the model are as follows: $E_l = 30000$ MPa, $B_{1l} = 5 \times 10^{-5}$ , $B_{2l} = 1.2 \times 10^{-13}$, $B_{3l} = 3 \times 10^{-5}$ , $m_d = 4$ , $m_l = 5$ , $m_g = 6$ , $\beta_d = 0.1$ , $\beta_l = 0.2$ , $\beta_g = 0.3$ , $n = 0.5$ , $n_1 = 0.5$ , $n_2 = 0.5$ , $n_3 = 0.5$ , $f = 0.6$ , $f_1 = 0.6$ , $f_2 = 0.6$ , $f_3 = 0.6$ , $n_m = 0.7$ , $f_m = 0.7$ , $n_\beta = 0.8$ and $f_\beta = 0.8$ .

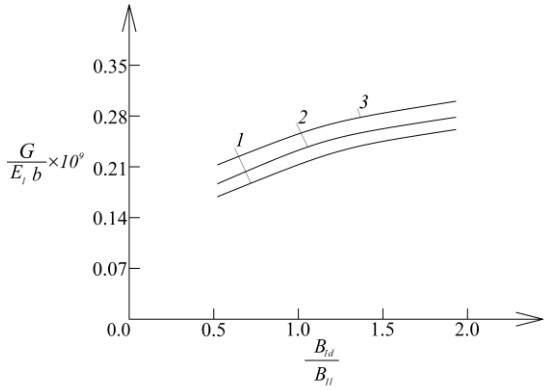


Figure 4. The non-dimensional SERR versus $B_{1d} / B_{1l}$ ratio (curve 1 - at $B_{1g} / B_{1l} = 0.5$ , curve 2 - at $B_{1g} / B_{1l} = 1.0$ and curve 3 - at $B_{1g} / B_{1l} = 2.0$ )

The influence of the time on the lengthwise fracture is examined in Fig. 2 where the SERR in non-dimensional form is presented as a function of the time at three $E_d / E_l$ ratios. The ratio, $E_d / E_l$, is a measure of the variation of $E$ in the direction of thickness.

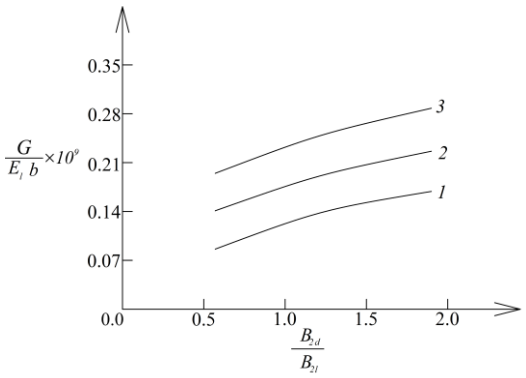


Figure 5. The non-dimensional SERR versus $B_{2d} / B_{2l}$ ratio (curve 1 - at $B_{2g} / B_{2l} = 0.5$ , curve 2 - at $B_{2g} / B_{2l} = 1.0$ and curve 3 - at $B_{2g} / B_{2l} = 2.0$ )

The time in Fig. 2 is in non-dimensional form (the formula, $t_N = t\beta_l$ , is used). From Fig. 2 it is evident that SERR rises over time. This rise is conditioned by the continuous growth of strains because of the creep in the frame. The variation of $E$ along the frame thickness also significantly affects the SERR (Figure 2 indicates that SERR reduces when ratio, $E_d / E_l$ , grows, which is a result of increasing of frame stiffness).

How the location of the lengthwise crack along the thickness of the frame cross-section affects the lengthwise fracture is studied next. In this relation, the SERR in non-dimensional form is presented as a

function of $h_1/h$ ratio in Fig. 3 at three $E_g/E_l$ ratios. The curves in Fig. 3 show that the SERR is maximal when the crack is located near the mid-thickness. Concerning the influence of $E_g/E_l$ ratio, the curves in Fig. 3 show that the SERR reduces with rise of $E_g/E_l$ ratio, which is due to increase of stiffness.

The change of the SERR with rise of $B_{1d}/B_{1l}$ and $B_{1g}/B_{1l}$ ratios is also studied. In this relation, the SERR in non-dimensional form is presented in a function $B_{1d}/B_{1l}$ ratio in Fig. 4 at three $B_{1g}/B_{1l}$ ratios. It can be observed in Fig. 4 that the SERR grows with increasing of $B_{1d}/B_{1l}$ and $B_{1g}/B_{1l}$ ratios (this can be explained by decreasing of the frame thickness).

The effect of $B_{2d}/B_{2l}$ and $B_{2g}/B_{2l}$ ratios on the lengthwise fracture is analyzed. In this relation, analysis of the SERR are carried-out at various $B_{2d}/B_{2l}$ and $B_{2g}/B_{2l}$ ratios. The effect is illustrated in Fig. 5 where the SERR in non-dimensional form is presented in a function of $B_{2d}/B_{2l}$ ratio at three $B_{2g}/B_{2l}$ ratios. The curves in Fig. 5 indicate that the SERR grows with increasing of $B_{2d}/B_{2l}$ and $B_{2g}/B_{2l}$ ratios (this is consequence of reducing the frame stiffness).

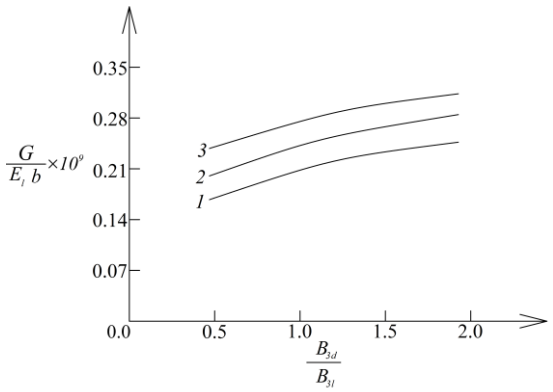


Figure 6. The non-dimensional SERR versus $B_{3d}/B_{3l}$ ratio (curve 1 - at $B_{3g}/B_{3l}=0.5$, curve 2 - at $B_{3g}/B_{3l}=1.0$ and curve 3 - at $B_{3g}/B_{3l}=2.0$)

An investigation of the influence of $B_{3d}/B_{3l}$ and $B_{3g}/B_{3l}$ ratios on the lengthwise fracture is also performed. For this purpose, the SERR at various $B_{3d}/B_{3l}$ and $B_{3g}/B_{3l}$ ratios is shown in Fig. 6 where the SERR in non-dimensional form is presented in a function of $B_{3d}/B_{3l}$ ratio at three $B_{3g}/B_{3l}$ ratios. It is evident from Fig. 6 that increase of $B_{3d}/B_{3l}$ and $B_{3g}/B_{3l}$ ratios result in growth of the SERR (the reason for this behavior is the frame stiffness decreasing).

## 4. Conclusion

1) It is observed that the SERR rises over time.

2) The investigation reveals that the SERR is maximal when the crack is located near the mid-thickness.

3) The analyses indicate that the SERR reduces with growing of $E_d/E_l$ and $E_g/E_l$ ratios.

4) The growth of $B_{1d}/B_{1l}$, $B_{1g}/B_{1l}$, $B_{2d}/B_{2l}$, $B_{2g}/B_{2l}$, $B_{3d}/B_{3l}$ and $B_{3g}/B_{3l}$ ratios result in rise of the SERR.

The practical application of the present research is in various analyses of fracture in frames hosting internal crack under creep. For instance, the research can be used to determine the critical time (this is the time after which a crack in a beam structure under constant load will begin to grow due to creep). To determine the critical time, we have to analyze the SERR – time relation and to obtain the time value at which SERR will become equal to the fracture toughness. The analysis of fracture in continuously inhomogeneous frames with internal lengthwise cracks during stress relaxation can be a topic of future work.

## References

1. B.N. Kumar, H. Singh, H.S. Nanda, eds. *Novel Applications of Functionally Graded Materials*. CRC Press, 2025. https://doi.org/10.1201/9781003656333
2. I. Meyer, L. Glitt, T. Ehlers. "Adjustment through Functionally Graded", *Innovative Produktentwicklung durch additive Fertigung: Innovative Product Development by Additive Manufacturing 2023* (2025): pp. 231-246, 2025. https://doi.org/10.1007/978-3-662-69327-8_15
3. R. Kumar, A. Agrawal, "Emerging Functionally Graded Materials for Bio-implant Applications—Design and Manufacturing", *In: Mahajan, A., Devgan, S., Zitoune, R. (eds) Additive Manufacturing of Bio-implants. Biomedical Materials for Multi-functional Applications*, Springer, Singapore, 2024. https://doi.org/10.1007/978-981-99-6972-2_9
4. R.F. Silva, P.G. Coelho, F.M. Conde, C.J. Almeida, A.L. Custódio, "Topology optimization of thermoelastic structures with single and functionally graded materials exploring energy and stress-based formulations", *Struct Multidisc Optim*, vol. 68, 11, 2025. https://doi.org/10.1007/s00158-024-03929-1
5. J. Toudehdehghan, W. Lim, K.E. Foo1, M.I.N. Ma'arof, J. Mathews, "A brief review of functionally graded materials", *MATEC Web of Conferences*, vol. 131, 03010, 2017. https://doi.org/10.1051/matecconf/201713103010
6. Y. Tokovyy, C.-C. Ma, "Axisymmetric Stresses in an Elastic Radially Inhomogeneous Cylinder Under Length-Varying Loadings", *J. Appl. Mech.*, vol. 83, no. 11, p. 111007, 2016.

http://doi.org/10.1115/1.4034459
7. K. Bousmaha, S.A. Belalia, S.M. Chorfi, A. Tounsi, M.A. Al-Osta, A.E. Alluqmani, "On the dynamic behavior of plates made of porous advanced materials reinforced with carbon nanotubes using a *p*-version of finite element method", *Mechanics Based Design of Structures and Machines*, pp. 1–30, 2025. https://doi.org/10.1080/15397734.2025.2534679
8. A. Tounsi, Z. Belabed, F. Bounouara, M. Balubaid, S.R. Mahmoud, A.A. Bousahla, A. Tounsi, "A finite element approach for forced dynamical responses of porous FG nanocomposite beams resting on viscoelastic foundations", *Int. J. Struct. Stab. Dyn.*, 2650078, 2024. https://doi.org/10.1142/S0219455426500781
9. S.A. Meftah, S.M. Aldosari, A. Tounsi, T. Cuong-Le, K.M. Khedher, A.E. Alluqmani, "Simplified homogenization technique for nonlinear finite element analysis of in-plane loaded masonry walls", *Engineering Structures*, vol. 306, 117822, 2024. https://doi.org/10.1016/j.engstruct.2024.117822
10. N. E. Dowling, *Mechanical behaviour of materials*, Pearson, 2011.
11. J. Chen, S. Tu, S. "Creep fracture parameters of functionally graded coating", *Journal of the Chinese Institute of Engineers*, vol. 27, pp. 805–812, 2004. https://doi.org/10.1080/02533839.2004.9670931
12. H. Guo, W. Tang, X. Tong, "Analysis of the Constraint-Based Creep Fracture Behavior of a Reactor Pressure Vessel with a Surface Crack Under Extreme High Temperature", *Nuclear Science and Engineering*, 1–11, 2025. https://doi.org/10.1080/00295639.2025.2503124
13. S. Yu, W. Dong, F.M. Xu, M.B. Fu, Y. Tan, "Effects of heat treatment on the creep crack growth behavior in Al/Al-4wt% Cu functionally graded material", *Adv. Mater. Res.*, vol. 711, pp. 81-86, 2013. https://doi.org/10.4028/www.scientific.net/AMR.711.81
14. V. Rizov, "Non-linear fracture in bi-directional graded shafts in torsion", *Multidiscipline Modeling in Materials and Structures*, vol. 15, pp. 156-169, 2018. https://doi.org/10.1108/MMMS-12-2017-0163
15. V. Rizov, "Viscoelastic inhomogeneous beam under time-dependent strains: A longitudinal crack analysis", *Advances in computational design: an International Journal*, vol. 6, no. 2, pp. 153-168, 2021 https://doi.org/10.12989/acd.2021.6.2.153153
16. V. Rizov, "Analysis of Two Lengthwise Cracks in a Viscoelastic Inhomogeneous Beam Structure", *Engineering Transactions*, vol. 68, pp. 397-415, 2020. https://doi.org/10.24423/EngTrans.1214.20201125
17. D. Broek, "Elementary engineering fracture mechanics," Springer, 1986.